Available online at www.sciencedirect.com
ScienceDirect
Atmospheric Environment 42 (2008) 4964–4975
ATMOSPHERIC ENVIRONMENT
www.elsevier.com/locate/atmosenv

Further studies of flow and reactive pollutant dispersion in a street canyon with bottom heating

Yoon-So Kang[a], Jong-Jin Baik[a,*], Jae-Jin Kim[b]

[a]School of Earth and Environmental Sciences, Seoul National University, Seoul 151-742, Republic of Korea
[b]Department of Environmental Atmospheric Sciences, Pukyong National University, Busan 608-737, Republic of Korea

Received 21 September 2007; received in revised form 9 February 2008; accepted 12 February 2008

Abstract

This study numerically investigates how flow and reactive pollutant dispersion in a street canyon with a canyon aspect ratio of one vary with the street-bottom heating intensity. For this, numerical simulations are performed over a wide range of street-bottom heating intensities ($\Delta T = 0$–$15\,^{\circ}C$ in $1\,^{\circ}C$ intervals) using a Reynolds-averaged Navier–Stokes equations (RANS) model with NO–NO_2–O_3 photochemistry. The pollutants NO and NO_2 are emitted from near the street bottom in the presence of background O_3.

A primary vortex is formed in the street canyon in all the simulated cases, but the location of the vortex center at the cross-canyon plane becomes quasi-stationary or meanders in the street canyon, depending on the street-bottom heating intensity. The time series of the street canyon-averaged NO concentration at the cross-canyon plane exhibits a quasi-steady, oscillatory, or fluctuating pattern, depending on the street-bottom heating intensity. As the street-bottom heating intensity increases, the averaged NO and NO_2 concentrations tend to decrease and the magnitude of the roof-level area-integrated and time-averaged vertical mean (turbulent) flux between $\Delta T = 2$ and $13\,^{\circ}C$ tends to increase (decrease). Some peculiar features are found in the cases of $\Delta T = 11$, 12, and $13\,^{\circ}C$ in which there are strong downward motion near the downwind building wall, downward motion below the roof level near the upwind building wall, and strong reverse flow in the lower region of the street canyon. Moreover, the vortex center is shifted toward the upwind building wall and does not meander in the street canyon after a certain period of time. Following the downward motions below the roof level, the O_3-containing ambient air is considerably entrained into the street canyon, resulting in a large increase in the O_3 concentration in the street canyon. In the cases of $\Delta T = 11$, 12, and $13\,^{\circ}C$, the magnitude of the vertical mean flux is larger than that of the vertical turbulent flux. The direct effect of the inhomogeneous temperature distribution on the O_3 concentration via the temperature-dependent photolysis rate and reaction rate constant increases with the street-bottom heating intensity, although the averaged fractional difference in O_3 concentrations is small.

Keywords: RANS model; Street canyon; Street-bottom heating intensity; Street canyon flow; Reactive pollutant dispersion; NO–NO_2–O_3 photochemistry

1. Introduction

In the past two decades, interest in the study of flow and pollutant dispersion in urban street canyons has rapidly increased. To gain a better

*Corresponding author. Tel.: +82 2 880 6990; fax: +82 2 883 4972.
E-mail address: jjbaik@snu.ac.kr (J.-J. Baik).

1352-2310/$ - see front matter © 2008 Elsevier Ltd. All rights reserved.
doi:10.1016/j.atmosenv.2008.02.013

understanding of street canyon flow and pollutant dispersion and also to provide some practical guidelines regarding urban air quality and urban planning, extensive studies have been conducted through field measurements (e.g., DePaul and Sheih, 1986; Eliasson et al., 2006), wind tunnel or water tank experiments (e.g., Kastner-Klein and Plate, 1999; Baik et al., 2000), and numerical model simulations (e.g., Lee and Park, 1994; Liu and Barth, 2002). These and other studies have identified many factors that affect flow and pollutant dispersion in street canyons, including the ambient wind speed and direction, building geometry, thermal stratification, and so on.

An important factor that should be taken into account is the street-bottom or building-wall heating by incoming solar radiation. The thermal effects on flow and pollutant dispersion in street canyons have been studied through wind tunnel experiments (Uehara et al., 2000; Kovar-Panskus et al., 2002; Richards et al., 2006) and numerical model simulations. Most of the numerical studies of the thermal effects have been confined to two-dimensional simulations using either steady Reynolds-averaged Navier–Stokes equations (RANS) models (Xie et al., 2006, 2007) or unsteady RANS models (Sini et al., 1996; Kim and Baik, 1999, 2001). The two-dimensional steady or unsteady model simulation results are validated using wind tunnel experimental data, showing the capability of RANS models in simulating thermal field in street canyons (Kim and Baik, 2001; Xie et al., 2006, 2007). The three-dimensional numerical studies of the thermal effects are few in literature. Using a three-dimensional, steady RANS model, Tsai et al. (2005) examined the effects of street-bottom and building-wall heating on flow and pollutant dispersion in a street canyon with a height-to-width ratio of 0.8 and a length-to-width ratio of 3. They showed that the vortex line that connects the centers of the cross-sectional vortices meanders in the street canyon.

Heretofore, almost all the studies of pollutant dispersion in street canyons have considered passive, inert pollutants. However, most pollutants in the atmosphere are chemically reactive. Baker et al. (2004) examined reactive pollutant dispersion in a street canyon with an aspect ratio of one using a three-dimensional, large-eddy simulation (LES) model. They included the following simple photochemistry involving NO, NO_2, and O_3:

$$NO_2 + h\nu \rightarrow NO + O, \quad (1)$$

$$O + O_2 + M \rightarrow O_3 + M, \quad (2)$$

$$O_3 + NO \rightarrow NO_2 + O_2. \quad (3)$$

In Baker et al. (2004), the thermodynamic energy equation is not included. Baik et al. (2007) developed a three-dimensional, unsteady RANS model with a thermodynamic energy equation and the above photochemical processes and examined flow and reactive pollutant dispersion in a street canyon with an aspect ratio of one in the presence of street-bottom heating. The street-bottom heating intensity was specified as $\Delta T = 5\,^{\circ}C$. They showed that at the cross-sectional plane the horizontal and vertical locations of the vortex center and the canyon-averaged temperature and reactive pollutant concentrations oscillate with time and that the inhomogeneous temperature distribution affects the O_3 concentration to some extent due to the temperature-dependent photolysis rate and reaction rate constant.

This study extends our previous study (Baik et al., 2007) to investigate how flow and reactive pollutant dispersion in a street canyon vary with the street-bottom heating intensity. For this, numerical simulations are performed over a wide range of street-bottom heating intensities.

2. Experimental design

The numerical model used in this study is the computational fluid dynamics (CFD) model developed by Baik et al. (2007). The numerical model is a RANS model with the re-normalization group (RNG) k–ε turbulence closure scheme and contains transport equations for NO, NO_2, and O_3 with the simple photochemistry described in (1)–(3). The photolysis rate of NO_2 in (1), J_{NO_2}, and the rate constant for reaction (3), k_1, are functions of temperature (Shetter et al., 1988; Baker et al., 2004; Baik et al., 2007). The governing equations are solved numerically in a staggered grid system using a finite volume method.

The building configuration considered in this study imitates an infinitely long street canyon (Fig. 1); this was also used in Baik et al. (2007). The coordinate origin is located at the center of the street bottom with x being the cross-canyon direction, y the along-canyon direction, and z the vertical direction. The ambient wind blows perpendicular to the along-canyon direction. The computational domain size is $40\,m \times 50\,m \times 60\,m$ in the x-,

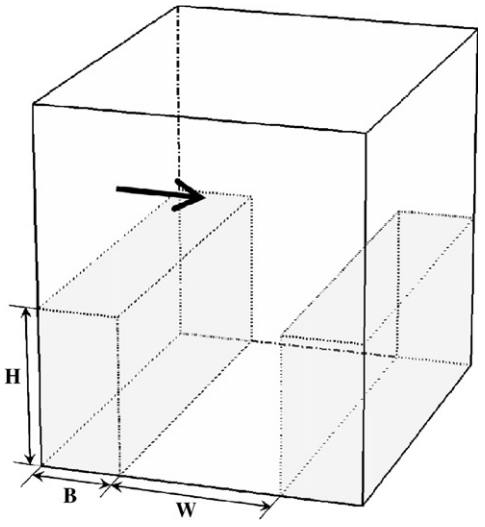

Fig. 1. The computational domain and building configuration. H is the building height and W is the width between two buildings. The ambient wind direction is perpendicular to the along-canyon direction and the street-bottom heating is applied to the entire street bottom. The reactive pollutants NO and NO_2 are emitted at the lowest grid points (area source).

y-, and z-direction. The model domain is composed of two equal-sized buildings with a building height H of 20 m and a street with a width between the two buildings W of 20 m. Thus, the canyon aspect ratio H/W is one. B in Fig. 1 is 10 m. The grid sizes in the x- and y-direction are uniform with $\Delta x = 0.5$ m and $\Delta y = 1$ m, respectively, and the grid size in the z-direction is uniform up to $z = 32$ m with $\Delta z = 0.5$ m and then increases with an expansion ratio of 1.1. The size of the street canyon is $20\,\text{m} \times 50\,\text{m} \times 20\,\text{m}$. The time step used is 0.1 s and the model is integrated over 2 h.

This study considers a situation wherein the pollutants NO, NO_2, and O_3 react in the presence of NO and NO_2 emissions from automobiles and background O_3. The initialization method for the reactive pollutants follows that of Baker et al. (2004) and Baik et al. (2007). There is no emission during the first 30 min. For the next 30 min ($t = 30$–60 min), passive pollutants are emitted at a rate of $50\,\text{ppb}\,\text{s}^{-1}$ per grid cell from the grid cells nearest the street bottom ($z = 0.25$ m). The area of the emission source is $20\,\text{m} \times 50\,\text{m}$. At $t = 60$ min, the NO concentration is set as the passive pollutant concentration and the NO_2 concentration is set at one-tenth the NO concentration, and the O_3 concentration is calculated by the photostationary state relation, $[O_3] = J_{NO_2}[NO_2]/k_1[NO]$, where the NO concentration is non-zero. When the NO concentration is zero (practically a very small value), the O_3 concentration is specified as 20 ppb. For the next 1 h ($t = 60$–120 min), NO and NO_2 are emitted at rates of 50 and $5\,\text{ppb}\,\text{s}^{-1}$ per grid cell, respectively.

The street bottom is heated by incoming solar radiation. The initial air temperature is 25 °C and the temperature at the street bottom is fixed during the model integration. Numerical simulations are performed with different street-bottom heating intensities. The initial temperature difference between the street bottom and the air, hereinafter referred to as the street-bottom heating intensity (ΔT), changes from 0 to 15 °C in 1 °C intervals. At the inflow boundary, the air temperature is 25 °C and the ambient wind speed is given by a logarithmic profile. For further details of the CFD-chemistry model and the experimental design, see Baik et al. (2007).

Experimental data on the concentrations of reactive pollutants in street canyons are not available yet; therefore, the present coupled CFD-chemistry model cannot be validated. However, the present CFD model, with the chemistry part excluded, has been validated against the wind tunnel data of Uehara et al. (2000) in Baik et al. (2007). The accuracy of the present CFD model including the thermodynamic energy equation and the RNG k–ε turbulence closure scheme in simulating street canyon flows has been justified in Baik et al. (2007).

3. Results and discussion

Sixteen numerical simulations are performed with different street-bottom heating intensities ($\Delta T = 0$–15 °C in 1 °C intervals) and the simulation results are analyzed. Fig. 2 shows streamline and temperature fields at $y/H = -0.025$ and $t = 100$ min for $\Delta T = 8$, 13, and 15 °C. In all the three cases, a clockwise-rotating, primary vortex is formed in the street canyon and a small, counterclockwise-rotating vortex is produced near the bottom corner of the downwind building. Among the three cases, the location of the vortex center is closest to the upwind building wall when ΔT is 13 °C. An examination of the time evolution of the streamline field (not shown) showed that for $\Delta T = 8$ and 15 °C the location of the vortex center in the street canyon changes with time, while for $\Delta T = 13$ °C no change

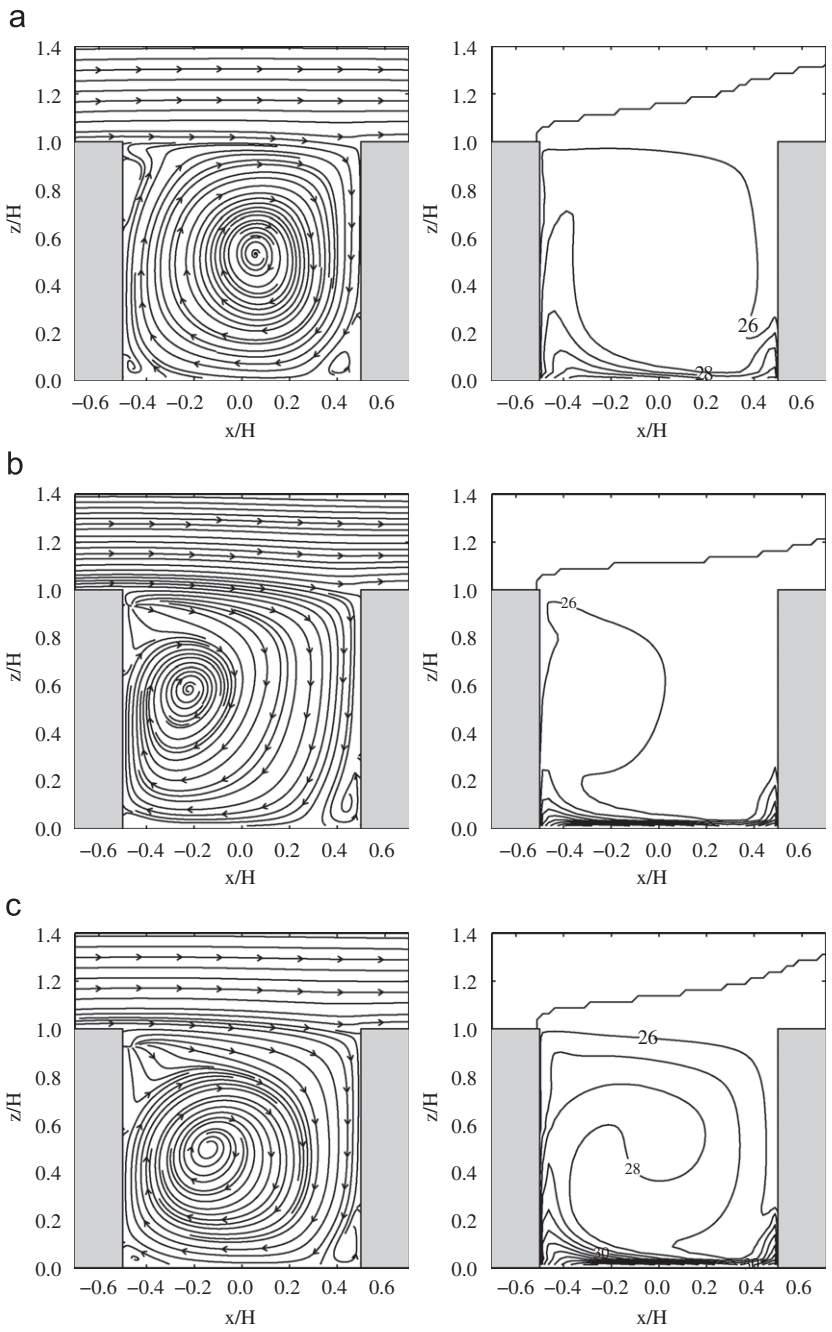

Fig. 2. Streamline (left column) and temperature (right column) fields at $y/H = -0.025$ and $t = 100$ min in the cases of $\Delta T =$ (a) 8 °C, (b) 13 °C, and (c) 15 °C. The contour interval in temperature fields is 1 °C.

in the location of the vortex center is observed after $t = 88$ min. The temperature near the upwind building wall is higher than that near the downwind building wall because of the heat transport by the primary vortex circulation. The temperature near the bottom corner of the downwind building is high. This is because in that region the small vortex transports heat toward the downwind building and then in the upward direction.

Fig. 3 shows the vertical profiles of the vertical velocity at the location $(x/H,\ y/H) = (-0.3875, -0.025)$, which is near the upwind building wall,

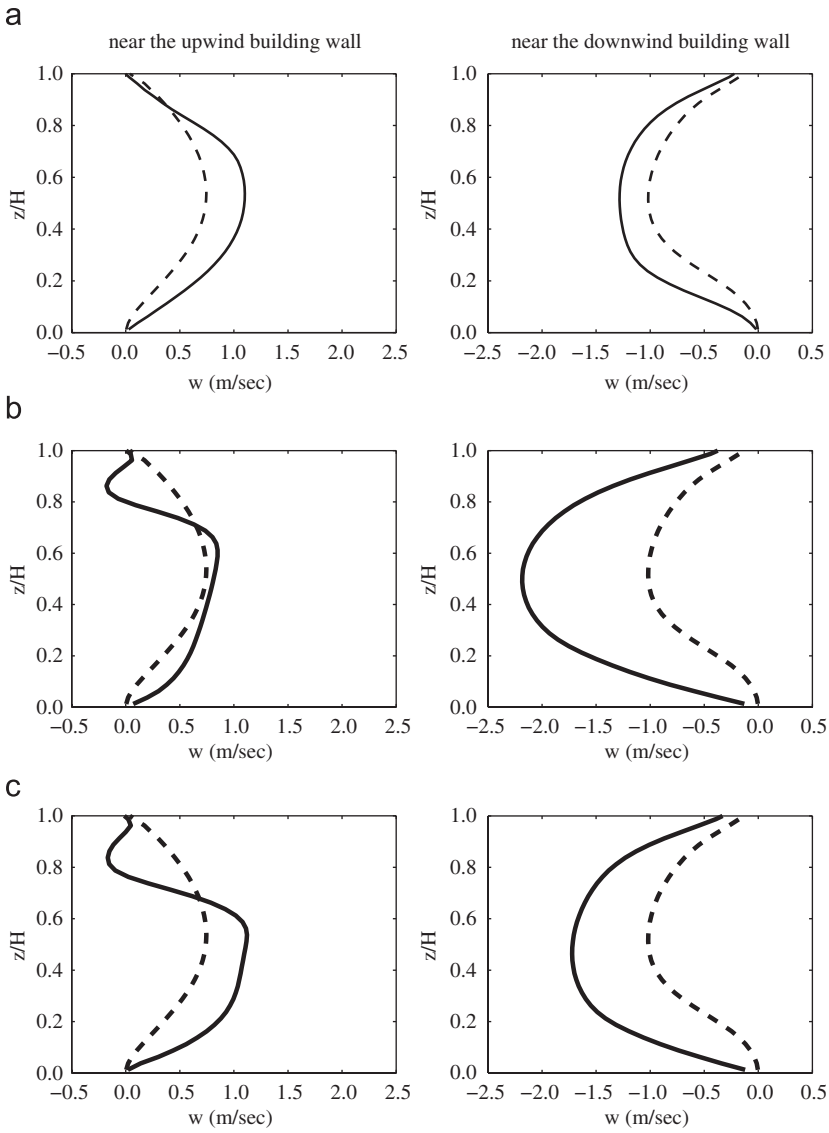

Fig. 3. Vertical profiles of the vertical velocity at $t = 100$ min in the cases of $\Delta T =$ (a) 8 °C, (b) 13 °C, and (c) 15 °C (solid lines) and in the no-heating case (dashed lines). Figures in the left and right columns are at $(x/H,\ y/H) = (-0.3875,\ -0.025)$ and $(x/H,\ y/H) = (0.3875,\ -0.025)$, respectively.

and also at the location $(x/H,\ y/H) = (0.3875,\ -0.025)$, which is near the downwind building wall, for $\Delta T = 8$, 13, and 15 °C. The selected time is $t = 100$ min. Note that the vertical profile of the vertical velocity for $\Delta T = 8$ and 15 °C changes with time as the vortex center meanders in the street canyon, while in the vertical profile for $\Delta T = 13$ °C almost no change occurs after $t = 94$ min. The downward motion near the downwind building wall is stronger in the street-bottom heating cases than in the no-heating case. For $\Delta T = 15$ °C, there is a downward motion in a region below the roof level, $0.775 \leqslant z/H \leqslant 0.950$, near the upwind building wall. The vertical profiles of the vertical velocity for $\Delta T = 13$ °C are similar to those for $\Delta T = 15$ °C, but the downward motion near the downwind building wall is stronger than that for $\Delta T = 15$ °C and about twice as strong as that for $\Delta T = 8$ °C. An analysis revealed that at the cross-canyon plane around the domain center the flow toward the upwind building wall in the lower region of the street canyon is much stronger for $\Delta T = 13$ °C than for $\Delta T = 8$ and 15 °C.

Fig. 4 shows the canyon- and time-averaged horizontal and vertical locations of the vortex

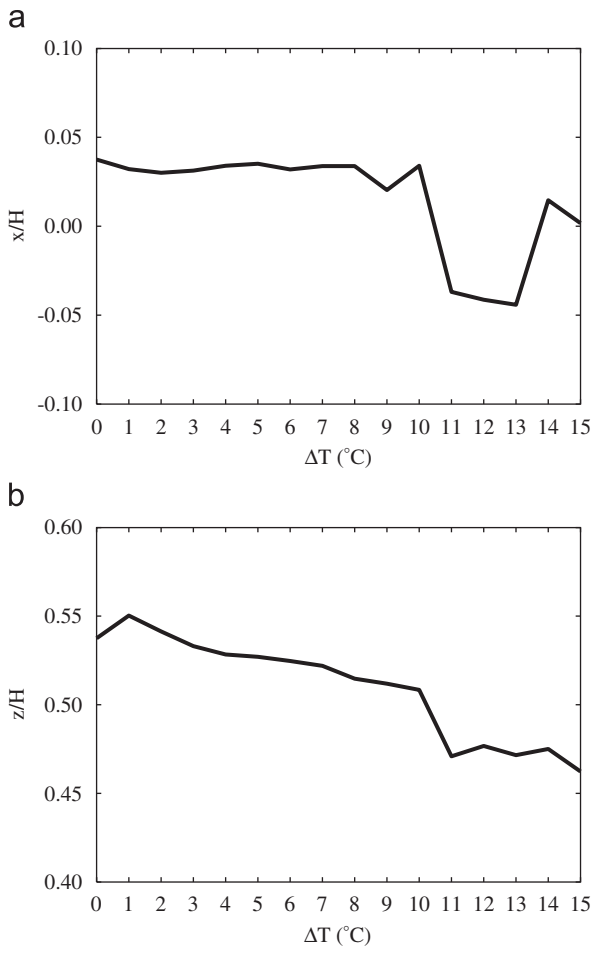

Fig. 4. Average (a) x-location and (b) z-location of the vortex center as a function of the street-bottom heating intensity. The average is taken over a canyon space of $-0.5 \leqslant x/H \leqslant 0.5$, $-1 \leqslant y/H \leqslant 1$, and $0 \leqslant z/H \leqslant 1$ and a time period of $60\,\text{min} \leqslant t \leqslant 120\,\text{min}$.

center as a function of the street-bottom heating intensity. The average is taken over a canyon space of $-0.5 \leqslant x/H \leqslant 0.5$, $-1 \leqslant y/H \leqslant 1$, and $0 \leqslant z/H \leqslant 1$ and a time period of $60\,\text{min} \leqslant t \leqslant 120\,\text{min}$. The canyon space of $-1.25 \leqslant y/H \leqslant -1.00$ and $1.00 \leqslant y/H \leqslant 1.25$ is excluded because x–z cross-sectional vortices do not clearly appear near the y-directional ends of the street canyon. The values of x/H are positive, that is, the averaged vortex center is located toward the downwind building wall from the canyon center $(x/H, z/H) = (0, 0.5)$, except for $\Delta T = 11$, 12, and 13 °C in which the averaged vortex center is shifted toward the upwind building wall. As the street-bottom heating intensity increases, the averaged vortex center tends to become lower (Fig. 4b). There is a relatively large change in the vertical location of the averaged vortex center when ΔT changes from 10 to 11 °C. Note that the location of the vortex center for $\Delta T = 13$ °C (Fig. 2b) differs from that of the averaged vortex center (Fig. 4) for $\Delta T = 13$ °C since the location of the center of x–z cross-sectional vortices varies in the along-canyon direction.

Baik et al. (2007) examined flow and reactive pollutant dispersion for $\Delta T = 5$ °C. Their analysis results show oscillatory patterns in the time series of the horizontal and vertical locations of the vortex center in the cross-canyon plane and the cross-canyon-averaged temperature and reactive pollutant concentrations. Thus, it would be intriguing to examine whether oscillatory patterns indeed appear at different values of street-bottom heating. This issue is addressed with the time series of street canyon-averaged NO concentration at $y/H = -0.025$ (x–z plane closest to the center of the street canyon) in the simulations with different street-bottom heating intensities (Fig. 5). The average is taken over $-0.5 \leqslant x/H \leqslant 0.5$ and $0 \leqslant z/H \leqslant 1$. A spectral analysis is also performed using the time-series data to identify the dominant oscillation peaks. For $\Delta T = 0$ °C, the averaged NO concentration is virtually constant with time (dashed lines in Fig. 5). For $\Delta T = 1$ °C, there is very little fluctuation in the averaged NO concentration. For $\Delta T = 2$ and 3 °C, oscillatory patterns are observed, but their amplitudes are small. For $\Delta T = 4$ and 5 °C, a dominant oscillation period of about 15 min is observed with appreciable amplitudes. For $\Delta T = 6$, 7, 8, 9, and 10 °C, the time series exhibit different oscillation or fluctuation patterns, but there is no obvious trend between the street-bottom heating intensity and the oscillation or fluctuation pattern. For $\Delta T = 7$ °C, the dominant oscillation period at $y/H = -0.025$ is 10 min. It is very interesting to note that there are absolutely no oscillations or fluctuations for $\Delta T = 11$, 12, and 13 °C. For $\Delta T = 14$ and 15 °C, some oscillatory patterns appear from $t = 60$ min to about 90 min. Fig. 5 indicates that the time-evolution pattern of the reactive pollutant concentration strongly depends on the degree of street-bottom heating. As mentioned in the case of $\Delta T = 5$ °C (Baik et al., 2007), the oscillation patterns in the time series are not due to the nonlinear reactive chemical processes but stem from the dynamic characteristics of flow in the presence of street-bottom heating.

To examine the collective effects of street-bottom heating on reactive pollutant dispersion in the street

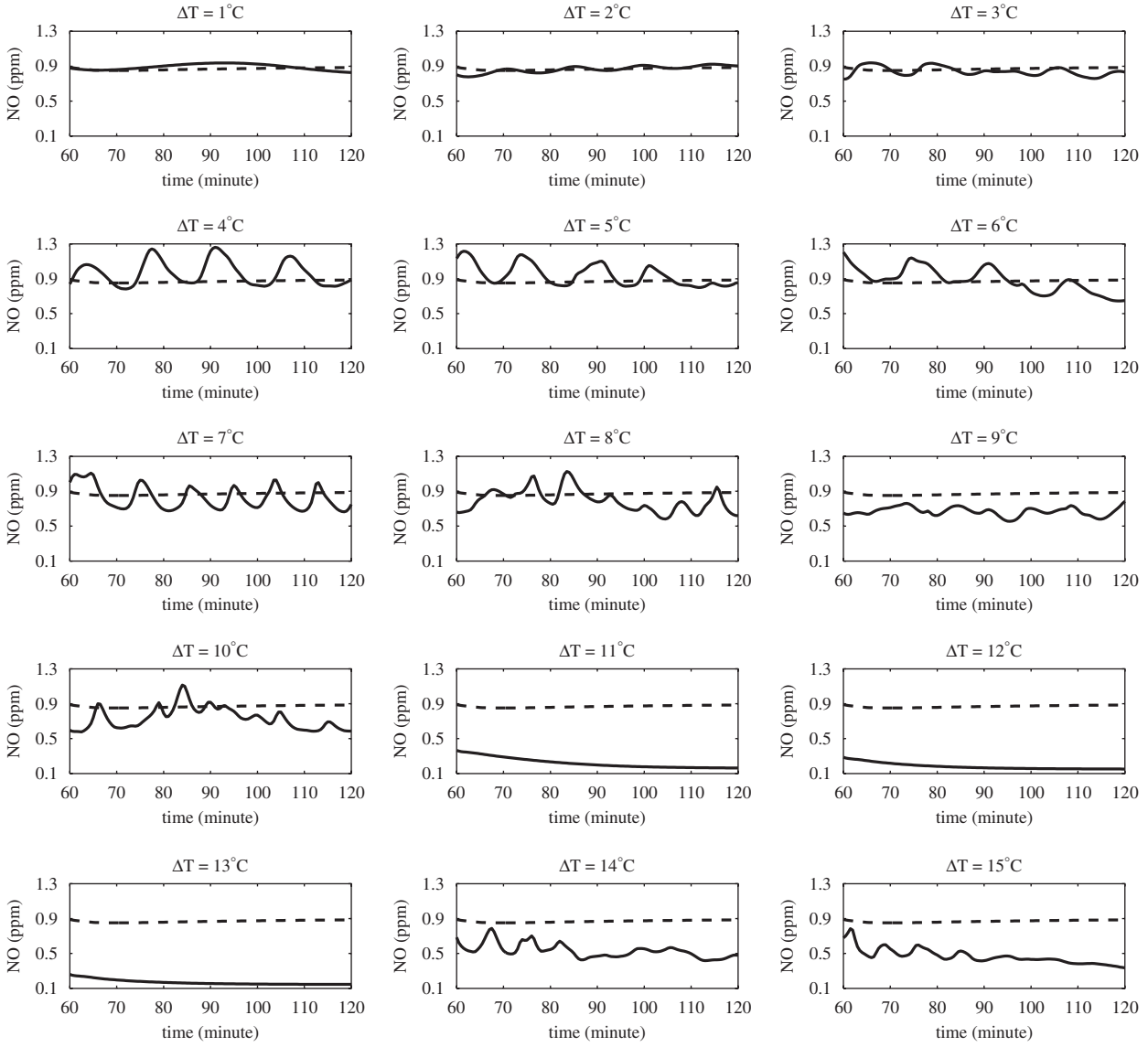

Fig. 5. Time series of the street canyon-averaged NO concentration at $y/H = -0.025$ in the cases of $\Delta T = 1$–15 °C (solid lines). Also, the time series in the no-heating case ($\Delta T = 0$ °C) is plotted in dashed lines in each figure.

canyon, the canyon- and time-averaged temperature and reactive pollutant concentrations are presented in Fig. 6 as a function of the street-bottom heating intensity. The average is taken over a canyon space of $-0.5 \leqslant x/H \leqslant 0.5$, $-1.25 \leqslant y/H \leqslant 1.25$, and $0 \leqslant z/H \leqslant 1$ and a time period of 60 min $\leqslant t \leqslant$ 120 min. As the street-bottom heating intensity increases, the averaged temperature increases gradually up to $\Delta T = 10$ °C, shows a slight decrease from $\Delta T = 10$ to 11 °C, and then increases with a (relatively) large rise from $\Delta T = 13$ to 14 °C. The averaged NO and NO_2 concentrations increase from $\Delta T = 1$ to 2 °C, decrease up to $\Delta T = 13$ °C with a large decrease from $\Delta T = 10$ to 11 °C, and then show a large increase from $\Delta T = 13$ to 14 °C and a decrease. The averaged O_3 concentration slightly increases from $\Delta T = 2$ to 10 °C, increases greatly from $\Delta T = 10$ to 13 °C, and then shows a large decrease from $\Delta T = 13$ to 14 °C and an increase. Fig. 6 shows that the averaged NO and NO_2 concentrations tend to decrease as the street-bottom heating intensity increases. Note that NO and NO_2 are emitted from near the street bottom. It is observed that the averaged NO and NO_2

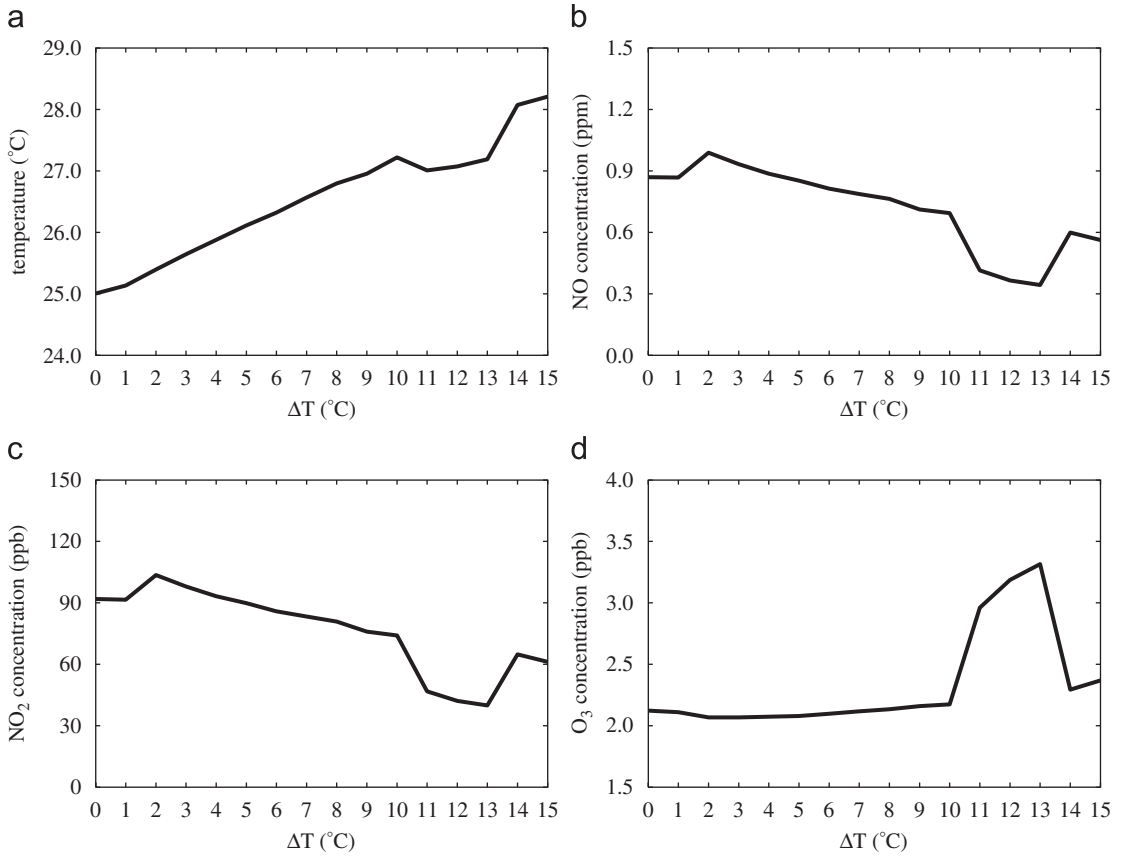

Fig. 6. Canyon- and time-averaged (a) temperature, (b) NO concentration, (c) NO_2 concentration, and (d) O_3 concentration as a function of the street-bottom heating intensity. The average is taken over a canyon space of $-0.5 \leqslant x/H \leqslant 0.5$, $-1.25 \leqslant y/H \leqslant 1.25$, and $0 \leqslant z/H \leqslant 1$ and a time period of $60\,\text{min} \leqslant t \leqslant 120\,\text{min}$.

concentrations in the presence of bottom heating are lower than those in the no-heating case when ΔT is larger than 5 °C, although the differences are not large when ΔT is less than 5 °C. This implies that the street canyon flow in the presence of bottom heating is not always more effective than that in the absence of bottom heating in lowering the in-canyon concentrations of pollutants that are emitted from near the street bottom.

To examine the individual contributions of the roof-level mean and turbulent fluxes to the escape of reactive pollutants from the street canyon, the area-integrated and time-averaged vertical mean and turbulent fluxes of the pollutant NO are presented as a function of the street-bottom heating intensity in Fig. 7. The area integration is taken over an area of $-0.5 \leqslant x/H \leqslant 0.5$ and $-1.25 \leqslant y/H \leqslant 1.25$ at the roof level ($z/H = 1$) and the time average is taken over a time period of $60\,\text{min} \leqslant t \leqslant 120\,\text{min}$. Here, the vertical mean and turbulent fluxes of NO are expressed by

$$F_m = CW, \tag{4}$$

$$F_t = \overline{cw} = -K_c \frac{\partial C}{\partial z}, \tag{5}$$

respectively, where C is the mean NO concentration, c the fluctuation from C, W the mean vertical velocity, w the fluctuation from W, and K_c the eddy diffusivity of NO. F_m and F_t are integrated over the area and then time-averaged over the time period. Fig. 7 shows that the calculated vertical mean and turbulent fluxes in all the cases are positive (except for the negligibly small negative values of the vertical mean flux for $\Delta T = 0$, 1, and 2 °C), indicating that both the vertical mean and turbulent fluxes at the roof level act to remove pollutants from the street canyon. Between $\Delta T = 2$ and 13 °C, the magnitude of the vertical mean (turbulent) flux tends to increase (decrease) as the street-bottom

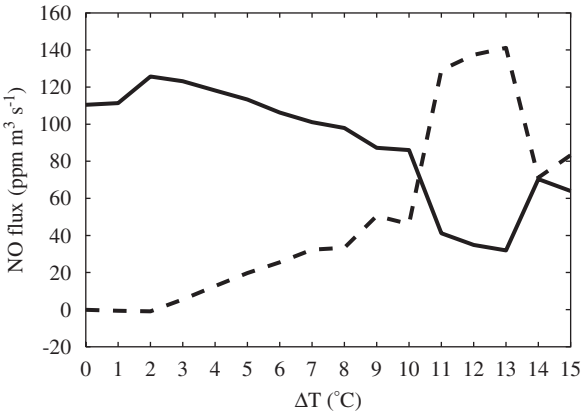

Fig. 7. Area-integrated and time-averaged vertical mean (dashed line) and turbulent (solid line) fluxes of NO as a function of the street-bottom heating intensity. The area integration is taken over an area of $-0.5 \leqslant x/H \leqslant 0.5$ and $-1.25 \leqslant y/H \leqslant 1.25$ at the roof level ($z/H = 1$) and the time average is taken over a time period of $60\,\text{min} \leqslant t \leqslant 120\,\text{min}$.

heating intensity increases. It is observed that from $\Delta T = 0$ to about 8 °C the magnitude of the vertical turbulent flux is much larger than that of the vertical mean flux and that up to $\Delta T \sim 10$ °C the difference in magnitude between the vertical mean and turbulent fluxes tends to decrease with increasing street-bottom heating intensity. When $\Delta T = 11$, 12, and 13 °C, the magnitude of the vertical mean flux is larger than that of the vertical turbulent flux.

It is interesting to observe that there are some peculiar features for $\Delta T = 11$, 12, and 13 °C, as compared with the other cases. In these cases ($\Delta T = 11$, 12, and 13 °C), there are strong downward motion near the downwind building wall, downward motion below the roof level near the upwind building wall, and strong reverse flow in the lower region of the street canyon. Moreover, the vortex center is shifted toward the upwind building wall and it does not meander in the street canyon after a certain period of time. Following the downward motions below the roof level, the O_3-containing ambient air is significantly entrained into the street canyon, resulting in a large increase in the O_3 concentration in the street canyon (Fig. 6d). On the other hand, in association with the primary vortex circulation, NO and NO_2 (their sources are near the street bottom) are distributed in a layer close to the street bottom due to the strong reverse flow, transported upward near the upwind building wall to the height at which the upward motion encounters the downward motion (Fig. 2b), and then transported toward the downwind building. Accordingly, in the presence of the strong downward motion in the upper region of the street canyon, the pollutants NO and NO_2 return to the street bottom, making it relatively difficult for them to escape from the street canyon. Nevertheless, the averaged NO and NO_2 concentrations in the street canyon are reduced. An analysis of the outward transport of reactive pollutants revealed that this is because the street canyon flow for $\Delta T = 11$, 12, and 13 °C is directed toward the y-directional ends of the street canyon with the horizontal velocity being stronger than that in the other cases and then exits the street canyon there.

The numerical simulations with a wide range of street-bottom heating intensities by Kim and Baik (2001) show that neither the peculiar features as in the cases of $\Delta T = 11$, 12, and 13 °C in the present study nor the oscillation/fluctuation patterns appear in two dimensions. The two-dimensional, time-dependent RANS models produce quasi-steady mean flows in the presence of street-bottom heating (Sini et al., 1996; Kim and Baik, 1999, 2001). However, this study shows that the three-dimensional, time-dependent RANS model can produce unsteady mean flows in the presence of street-bottom heating. These results indicate that in the presence of street-bottom heating quasi-steady mean flows in two dimensions can be unsteady in three dimensions. This is found to be an important aspect of flows simulated in three dimensions in the presence of heating.

Baik et al. (2007) calculated the fractional difference in reactive pollutant concentrations, defined in Eq. (6), to quantify the effect of the inhomogeneous temperature distribution on the reactive pollutant concentration in a street canyon due to the temperature-dependent photolysis rate J_{NO_2} and reaction rate constant k_1.

$$D = \left(\frac{C_0}{C_T} - 1\right) \times 100. \tag{6}$$

Here, C_0 is the reactive pollutant concentration in a simulation performed using J_{NO_2} and k_1 evaluated at 25 °C and C_T is the reactive pollutant concentration in a simulation performed using temperature-dependent J_{NO_2} and k_1. To calculate D, fifteen additional numerical simulations are performed with constant J_{NO_2} and k_1. Fig. 8 shows the fractional difference in O_3 concentrations averaged over the entire street canyon and the total integration time of reactive pollutants ($60\,\text{min} \leqslant t \leqslant 120\,\text{min}$) as

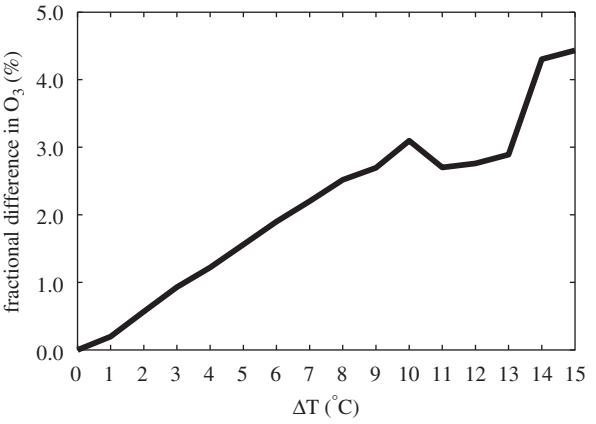

Fig. 8. Canyon- and time-averaged fractional difference in O_3 concentrations as a function of the street-bottom heating intensity. The average is taken over a canyon space of $-0.5 \leqslant x/H \leqslant 0.5$, $-1.25 \leqslant y/H \leqslant 1.25$, and $0 \leqslant z/H \leqslant 1$ and a time period of $60\,\text{min} \leqslant t \leqslant 120\,\text{min}$.

a function of the street-bottom heating intensity. The averaged fractional difference is positive, indicating that the O_3 concentration simulated using constant J_{NO_2} and k_1 is higher than that simulated using temperature-dependent J_{NO_2} and k_1. As the street-bottom heating intensity increases, the averaged fractional difference increases, except when $\Delta T = 11$, 12, and 13 °C. There is a decrease from $\Delta T = 10$ to 11 °C and a substantial increase from $\Delta T = 13$ to 14 °C. The abrupt decrease in the averaged fractional difference for $\Delta T = 11$, 12, and 13 °C is related to the abrupt increase in the O_3 concentration (Fig. 6d). Fig. 8 indicates that the inhomogeneous temperature distribution affects the reactive pollutant concentration via the temperature-dependent photolysis rate and reaction rate and that its influence tends to be large as the street-bottom heating becomes strong. The averaged fractional difference for O_3 is not large (e.g., 2.69% for $\Delta T = 9$ °C), but the fractional difference can be large, depending on the location and time. For example, the fractional difference is as large as 18.4% at $(x/H, y/H, z/H) = (-0.2375, 0.525, 0.0125)$ and $t = 81$ min for $\Delta T = 15$ °C. The standard deviation of the fractional difference was also computed to examine the spatial and temporal variability of the fractional difference. Results showed that for each ΔT the standard deviation of the fractional difference is smaller than the averaged fractional difference and that the standard deviation of the fractional difference increases with increasing street-bottom heating intensity up to $\Delta T = 13$ °C and then a slight decrease and then increase follows.

4. Summary and further research

This study was performed to understand how flow and reactive pollutant dispersion in a street canyon vary as the street-bottom heating intensity changes. To achieve this objective, a coupled CFD-chemistry model was employed. Through numerical simulations and analyses, the variations in flow and reactive pollutant dispersion with the street-bottom heating intensity could be described. Interestingly, it was found that the variations are not monotonic and there are some peculiar features that appear over a certain range of street-bottom heating intensities.

An infinitely long street-canyon configuration (Fig. 1) was considered in this study. Note that the phrase "infinitely long street-canyon configuration" in this study implicitly means a large L/H (L: building length), although the buildings are truncated by the model y-lateral boundaries. To examine the effects of building or street canyon configuration on flow and reactive pollutant dispersion in the presence of street-bottom heating, numerical simulations are performed in a finitely long street-canyon configuration (Fig. 9).

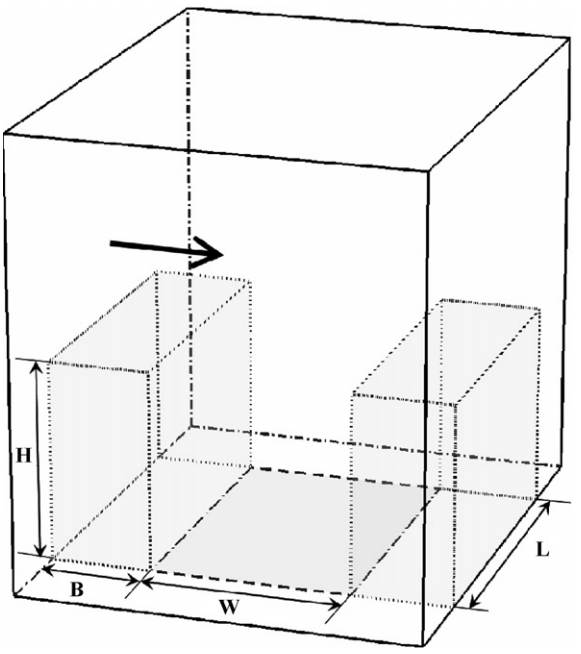

Fig. 9. The same as in Fig. 1 except for a finitely long street-canyon configuration.

The experimental design is the same as that described in Section 2 except that the building length in the along-canyon direction is 30 m (building is located between $-0.75 \leqslant y/H \leqslant 0.75$). Note that the heating is applied at all the street bottoms and the pollutants are emitted at $-0.5 \leqslant x/H \leqslant 0.5$ and $-0.75 \leqslant y/H \leqslant 0.75$. Fig. 10a–c shows the time series of the street canyon-averaged NO concentration at $y/H = -0.025$ in the cases of $\Delta T = 5$, 10, and 15 °C, respectively. There is no oscillation or fluctuation for $\Delta T = 5$ and 10 °C. This result is different from that in the infinitely long street-canyon configuration (Fig. 5). For $\Delta T = 15$ °C, the averaged NO concentration oscillates with time. Fig. 10d–g shows the canyon- and time-averaged temperature, NO concentration, NO_2 concentration, and O_3 concentration as a function of the street-bottom heating intensity, respectively. The averaged temperature tends to increase with increasing street-bottom heating intensity. The averaged NO and NO_2 concentrations increase up to $\Delta T = 5$ °C and then decrease gradually. The pattern of the averaged O_3 concentration is opposite to that of the averaged NO and NO_2 concentrations. This result is different from that in the infinitely long street-canyon configuration (Fig. 6).

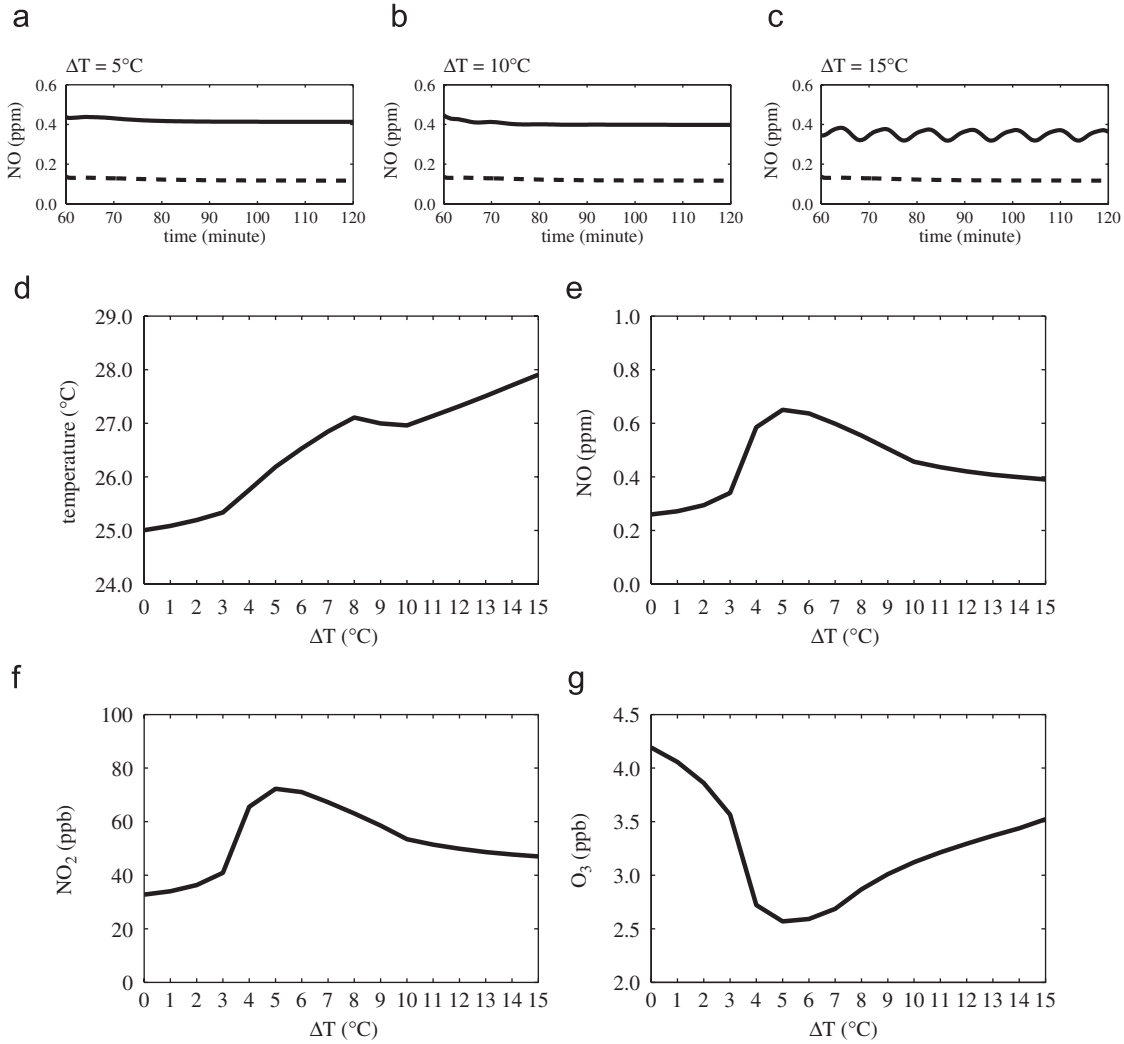

Fig. 10. (a–c) are the time series of the street canyon-averaged NO concentration at $y/H = -0.025$ in the cases of $\Delta T = 5$, 10, and 15 °C (solid lines) and in the no-heating case (dashed lines), respectively. (d–g) are the canyon- and time-averaged temperature, NO concentration, NO_2 concentration, and O_3 concentration as a function of the street-bottom heating intensity, respectively. The average is taken over a canyon space of $-0.5 \leqslant x/H \leqslant 0.5$, $-0.75 \leqslant y/H \leqslant 0.75$, and $0 \leqslant z/H \leqslant 1$ and a time period of 60 min $\leqslant t \leqslant$ 120 min. These are numerical simulation results in the finitely long street-canyon configuration.

Our numerical simulation results indicate that variations in flow and reactive or passive pollutant dispersion with the street-bottom heating intensity strongly depend on building or street-canyon configuration. A further systematic investigation for various building or street-canyon configurations is needed. Also, a study is required to dynamically explain reasons for the variations in flow and pollutant dispersion with the street-bottom heating intensity.

Acknowledgments

The authors are very grateful to one of the reviewers for providing valuable comments on the original manuscript. This work was in part funded by the Korea Meteorological Administration Research and Development Program under Grant CATER 2006-2202.

References

Baik, J.-J., Park, R.-S., Chun, H.-Y., Kim, J.-J., 2000. A laboratory model of urban street-canyon flows. Journal of Applied Meteorology 39, 1592–1600.

Baik, J.-J., Kang, Y.-S., Kim, J.-J., 2007. Modeling reactive pollutant dispersion in an urban street canyon. Atmospheric Environment 41, 934–949.

Baker, J., Walker, H.L., Cai, X., 2004. A study of the dispersion and transport of reactive pollutants in and above street canyons—a large eddy simulation. Atmospheric Environment 38, 6883–6892.

DePaul, F.T., Sheih, C.M., 1986. Measurements of wind velocities in a street canyon. Atmospheric Environment 20, 455–459.

Eliasson, I., Offerle, B., Grimmond, C.S.B., Lindqvist, S., 2006. Wind fields and turbulence statistics in an urban street canyon. Atmospheric Environment 40, 1–16.

Kastner-Klein, P., Plate, E.J., 1999. Wind-tunnel study of concentration fields in street canyons. Atmospheric Environment 33, 3973–3979.

Kim, J.-J., Baik, J.-J., 1999. A numerical study of thermal effects on flow and pollutant dispersion in urban street canyons. Journal of Applied Meteorology 38, 1249–1261.

Kim, J.-J., Baik, J.-J., 2001. Urban street-canyon flows with bottom heating. Atmospheric Environment 35, 3395–3404.

Kovar-Panskus, A., Moulinneuf, L., Savory, E., Abdelqari, A., Sini, J.-F., Posant, J.-M., Robins, A., Toy, N., 2002. A wind tunnel investigation of the influence of solar-induced wall-heating on the flow regime within a simulated urban street canyon. Water, Air, and Soil Pollution: Focus 2, 555–571.

Lee, I.Y., Park, H.M., 1994. Parameterization of the pollutant transport and dispersion in urban street canyons. Atmospheric Environment 28, 2343–2349.

Liu, C.H., Barth, M.C., 2002. Large-eddy simulation of flow and scalar transport in a modeled street canyon. Journal of Applied Meteorology 41, 660–673.

Richards, K., Schatzmann, M., Leitl, B., 2006. Wind tunnel experiments modelling the thermal effects within the vicinity of a single block building with leeward wall heating. Journal of Wind Engineering and Industrial Aerodynamics 94, 621–636.

Shetter, R.E., Davidson, J.A., Cantrell, C.A., Burzynski Jr., N.J., Calvert, J.G., 1988. Temperature dependence of the atmospheric photolysis rate coefficient for NO_2. Journal of Geophysical Research 93, 7113–7118.

Sini, J.-F., Anquetin, S., Mestayer, P.G., 1996. Pollutant dispersion and thermal effects in urban street canyons. Atmospheric Environment 30, 2659–2677.

Tsai, M.-Y., Chen, K.-S., Wu, C.-H., 2005. Three-dimensional modeling of air flow and pollutant dispersion in an urban street canyon with thermal effects. Journal of the Air and Waste Management Association 55, 1178–1189.

Uehara, K., Murakami, S., Oikawa, S., Wakamatsu, S., 2000. Wind tunnel experiments on how thermal stratification affects flow in and above urban street canyons. Atmospheric Environment 34, 1553–1562.

Xie, X., Liu, C.-H., Leung, D.Y.C., Leung, M.K.H., 2006. Characteristics of air exchange in a street canyon with ground heating. Atmospheric Environment 40, 6396–6409.

Xie, X., Liu, C.-H., Leung, D.Y.C., 2007. Impact of building facades and ground heating on wind flow and pollutant transport in street canyons. Atmospheric Environment 41, 9030–9049.